CySP3-96 enables scalable, streamlined, and low-cost sample preparation for cysteine chemoproteomic applications

Flowreen Shikwana[1,2], Beeta S. Heydari[7], Samuel Ofori[1], Cindy Truong[2], Alexandra C. Turmon[1,2], Joelle Darrouj[2], Lara Holoidovsky[1], Jeffrey L. Gustafson[7], Keriann M. Backus[1,2,3,4,5,6]*

1. Biological Chemistry Department, David Geffen School of Medicine, UCLA, Los Angeles, CA, 90095, USA.
2. Department of Chemistry and Biochemistry, UCLA, Los Angeles, CA, 90095, USA.
3. Molecular Biology Institute, UCLA, Los Angeles, CA, 90095, USA.
4. DOE Institute for Genomics and Proteomics, UCLA, Los Angeles, CA, 90095, USA.
5. Jonsson Comprehensive Cancer Center, UCLA, Los Angeles, CA, 90095, USA.
6. Eli and Edythe Broad Center of Regenerative Medicine and Stem Cell Research, UCLA, Los Angeles, CA, 90095, USA.
7. Department of Chemistry and Biochemistry, San Diego State University, San Diego, CA. 92182, USA

*Keriann M. Backus, Biological Chemistry Department, David Geffen School of Medicine, UCLA, Los Angeles, CA, 90095, USA, E-mail: kbackus@mednet.ucla.edu.

Abstract

Cysteine chemoproteomic screening platforms are widely utilized for chemical probe and drug discovery campaigns. Chemoproteomic compound screens, which use a mass spectrometry-based proteomic readout, can interrogate the structure activity relationship (SAR) for thousands of proteins in parallel across the proteome. The versatility of chemoproteomic screens has been demonstrated across electrophilic, nucleophilic, and reversible classes of molecules. However, a key bottleneck that remains for these approaches is the low throughput nature of most established sample preparation workflows, which rely on many time-intensive and often error prone steps. Addressing these challenges, here we establish a novel workflow, termed CySP3-96, that pairs single-pot, solid-phase-enhanced, sample preparation (SP3) with a customized 96-well sample cleanup workflow to achieve streamlined multiplexed sample preparation. Our CySP3-96 method addresses prior volume limitations of SP3, which allows for seamless 96-well chemoproteomic sample preparation, including for large input amounts that are incompatible with prior methods. By deploying CySP3-96 to screen a focused set of 16 cysteine-reactive compounds, we identify 2633 total ligandable cysteines, including 21 not captured in CysDB. Chemoproteomic analysis of a pair of atropisomeric electrophilic kinase inhibitors reveals striking stereoselective cysteine

https://doi.org/10.26434/chemrxiv-2024-jm4n0 **ORCID:** https://orcid.org/0000-0001-8541-1404 Content not peer-reviewed by ChemRxiv. **License:** CC BY-NC-ND 4.0

ligandability for 67 targets across the proteome. When paired with our innovative budget friendly magnetic resin, CySP3-96 represents a versatile, low cost, and highly reproducible screening platform with widespread applications spanning all types of chemoproteomic studies.

Introduction

Mass spectrometry-based chemoproteomics has emerged as a powerful technology capable of pinpointing potential druggable sites proteome-wide. Illustrating the broad impact of chemoproteomics, screening platforms are now available to assess nearly all nucleophilic amino acid site chains[1], inclusive of cysteine[2–5], lysine[6,7], serine[8–10], tyrosine[11–13], methionine[14,15], glutamate and aspartate[16–18]. Cysteine remains a favored residue to target, due to its high nucleophilicity, important structural and functional roles within proteins, and proven therapeutic relevance, as exemplified by FDA-approved cysteine-reactive drugs such as the Gly12Cys KRAS inhibitors[19,20]. Thus, a key objective of cysteine chemoproteomic studies is to enable the discovery of scout or pathfinder molecules[3,21–37] for all potentially druggable, or "ligandable," cysteine residues.

Towards achieving this goal, chemoproteomic screening platforms apply the same general strategy. First, cells or lysates are treated with electrophilic compounds or vehicle, followed by capping of all unreacted cysteines with a pan-cysteine reactive probe, such as iodoacetamide alkyne (IAA) or iodoacetamide desthiobiotin (DBIA). After control and treatment groups are isotopically differentiated, either via heavy/light biotin-reagents[5,38] or with isobaric tags[21,39,40], samples are then subject to sequence specific proteolysis and enrichment on avidin resin along with multiple sample cleanup steps throughout this process. Compound-modified cysteines are then identified via LC-MS/MS based on compound-induced decreases in either precursor or reporter ion abundance. Demonstrating their broad utility, these workflows have now been widely implemented both by our group[3,38,40–43] and many others[4,21,39,44], enabling discovery of covalent tool compounds that engage a wide range of protein classes, spanning transcription factors[45], RNA binding proteins[35], kinases[36], proteasome regulators[34], proteases[3,46], and even classes of post-translationally modified cysteines[47].

One important consideration for chemoproteomic screens is library composition. As chemoproteomic screens remain comparatively low throughput, selection of a focused and diverse set of electrophilic fragments and more elaborated compounds has become a go-to strategy to maximize coverage of potential targets[2,44]. Alongside structural diversity, the addition of enantioenriched libraries to chemoproteomic screening decks provides added value to facilitate delineation of high confidence compound-cysteine interactions and on target phenotypes[28,34,45,48–51]. While a number of studies have now reported chemoproteomic datasets using pairs of enantioprobes, the target profile of compounds featuring other types of chirality remains largely unexplored. Atropisomerism is a conformational chirality that occurs when there is constrained rotation about a bond that results in the 'rotamers' being isolable enantiomers. Atropisomerism is becoming increasingly ubiquitous throughout modern drug discovery[52]. However, to the best of our knowledge, there have been no chemoproteomic studies for atropisomer pairs.

With the increasing availability of comparatively large 3200+ electrophilic compound libraries available for purchase and new straightforward chemistries for rapid electrophilic compound library synthesis[53], the number of easily accessible electrophilic compounds available to

https://doi.org/10.26434/chemrxiv-2024-jm4n0 **ORCID:** https://orcid.org/0000-0001-8541-1404 Content not peer-reviewed by ChemRxiv. **License:** CC BY-NC-ND 4.0

researchers far outstrips current throughput of chemoproteomic screening platforms, both in terms of sample preparation and data acquisition. Methodological innovations that result in streamlined sample preparation offer the potential to improve sample throughput. Many groups have developed approaches to address these issues, such as SP2 for rapid and reproducible proteomics[54], implementation of microflow LC-MS/MS analysis for improved reproducibility[55], development of intelligent acquisition software[56], and utilizing a label-free approach to speed up acquisition and throughput[57]. Transitioning from 1.5 mL microfuge tubes to 96-well plates is one approach to improve sample reproducibility and throughput, which allows for reduced manual sample manipulation, decreased points for human error, and compatibility with automation. Sample cleanup methods, such as in-stage tip (iST)[58], S-Trap[59], and single-pot, solid-phase-enhanced sample preparation (SP3)[60,61] are integral parts of most plate-based sample workflows, as illustrated by their applications to phosphoproteomics[62], clinical proteomics[63,64], identification of stereo-specific targets[45], and discovery of off target proteins[39]. Our recent work revealed that SP3 cleanup is well-suited to chemoproteomics, yielding improved coverage and benefitting from decreased input material[41,42]. SP3 cleanup is also featured in the recently reported TMT- and 96-well-plate-based chemoproteomic platform by Gygi and colleagues[21], and has been shown to have high reproducibility between experimental replicates[65], which further demonstrates the utility of SP3 in transitioning cysteine chemoproteomics to streamlined automated sample preparation.

Despite these considerable advances, several unaddressed challenges remain. First, as demonstrated by us and others[41,66], SP3 cleanup does not scale well, with decreased yields at larger input materials—this limitation is particularly relevant for less reactive chemical probes, for which more sample is required to achieve higher coverage and for compatibility with microflow acquisition methods that are distinguished by low failure rates compared to nanoflow[55,67]. Second, and looking beyond SP3-specific workflows, many cleanup methods are quite costly, hindering implementation for large-scale screening applications. And lastly, for chemoproteomics, the avidin-enrichment step remains a bottleneck for fully transitioning an entire workflow into a 96-well format, with most prior reports conducting peptide capture manually in plastic containers.

Here we report the CySP3-96 method, which implements an unprecedented scalable SP3 cleanup and a low cost SP3-alternative resin to enable robust and high coverage cysteine ligandability screens in a fully 96-well plate format. To establish CySP3-96, we first determined the source of the decreased coverage for SP3 samples generated with higher protein input, namely increased peptide concentration in the tryptic digest. We addressed this limitation by bypassing the SP3 peptide cleanup step entirely, which allowed us to maintain volumes compatible with deepwell plates. Benchmarking the CySP3-96 method to our established cysteine-SP3 platform, revealed comparable coverage together with at least a 90-minute per sample decrease in processing time with increasing time saved proportional to increase in the number of samples. These improvements allowed for high coverage screening in a 96-well plate format of 16 total known and novel electrophiles, including unprecedented atropisomeric compounds, which identified 2633 total ligandable cysteines, of which 21 have not been reported previously in CysDB[68]. Distinguished by scalability, low cost, and ease of implementation, we expect CySP3-96 to prove widely useful for a broad range of cysteine chemoproteomic applications.

https://doi.org/10.26434/chemrxiv-2024-jm4n0 **ORCID:** https://orcid.org/0000-0001-8541-1404 Content not peer-reviewed by ChemRxiv. **License:** CC BY-NC-ND 4.0

Results

Increased tryptic digest concentration fails to enable lower volume sample preparation. The first step to transition our cysteine chemoproteomic workflow into a more high throughput platform was to scale down the volumes of key steps of our established method. In our previous SP3-enabled cysteine chemoproteomic sample preparation workflow (**Figure 1A**) the maximum volume reached during SP3 cleanup is 4 mL, which far exceeds the maximum volume available for a 96-well plate (2 mL for a 96-well deep well plate)—this large volume is required during the acetonitrile (>95% v/v) peptide binding step that occurs after the on-SP3 tryptic digest (**Table S1**). Furthermore, the shaking steps required for peptide binding to beads also limits the volume allowed in a deep well plate, with excess volume leading to inadvertent mixing between wells during shaking. Thus, to transition our method from 1.5 mL microcentrifuge tubes to a plate format, we first focused on the scaledown of this step. Our goal was to decrease total volume to under 1 mL while maintaining high coverage, both in terms of peptide recovery and cysteine peptides identified.

We first postulated that scaledown could easily be achieved by implementing an ultra high concentration and low volume tryptic digest (15 µL), which would allow for the decrease in volume for the peptide binding step. We tested the impact of this scaledown for cysteine chemoproteomic samples prepared using our v1.0 workflow (**Figure 1A**) with varying trypsin digest volumes, for Jurkat whole cell lysate (200 µg total material) labeled with iodoacetamide alkyne (IAA) followed by click conjugation to biotin azide (**Figure S1**). Disappointingly, we observed a decrease in peptide recovery with increased digest concentration, dropping from an average of ~60% to ~30% at the highest concentrations (**Figure 1B**). Providing further evidence that the scaledown approach was not suitable, coverage of enriched biotinylated cysteine peptide spectral matches (PSMs) and unique cysteines identified also decreased dramatically (~50% loss), when the digest protein concentration exceeded 4 mg/mL (**Figure 1C** and **1D**). Alongside this decrease in cysteine peptide coverage, we also observed an increased capture of background peptides lacking cysteine-biotin modifications for higher digest concentrations (**Figure 1E**). This finding hints at the likelihood that peptide aggregation in higher digest concentrations may lead to more non-specific binding to neutravidin resin.

Bypassing peptide cleanup step enables high coverage and low volume chemoproteomics. Thwarted by the decreased coverage for our digest-scaledown strategy, we next opted to test whether the peptide cleanup step could be omitted while maintaining high coverage (**Figure 2A**). While our prior studies had indicated that SP3-cleanup is highly beneficial for increasing coverage by removing trace biotin contaminants[41,42], we were inspired by other well-established non-SP3-based chemoproteomic methods[69,70] that do not include a peptide-cleanup prior to avidin/streptavidin enrichment. Gratifyingly, no significant change in coverage was observed for samples prepared with the omission of the peptide cleanup step (**Figure 2B**). We term this new cysteine chemoproteomic workflow, which omits the peptide cleanup step on SP3 prior to avidin enrichment, workflow v2.0 and the original workflow outlined in Yan et al. 2021 as workflow v1.0. Further illustrating comparable performance, a substantial overlap for cysteines identified was observed when both workflows were done side by side (**Figure 2C**), and similar coverage when compared to CysDB annotations of identified cysteines[68] (**Figure 2D**). Notably,

https://doi.org/10.26434/chemrxiv-2024-jm4n0 **ORCID:** https://orcid.org/0000-0001-8541-1404 Content not peer-reviewed by ChemRxiv. **License:** CC BY-NC-ND 4.0

peptide neutravidin eluants were directly analyzed with no further cleanup—to ensure that samples contained no substantial residual contaminants from the tryptic digest, we incorporated additional resin washes during the neutravidin capture step (see methods). We observed no significant difference in the proportion of enriched modified peptides between the two workflows (**Figure S3**), indicating that the effect of directly enriching post-digest is negligible. The elimination of a peptide-cleanup step on SP3 beads cuts the sample preparation time by at least 90 minutes and minimizes sample loss by reducing sample transfer steps.

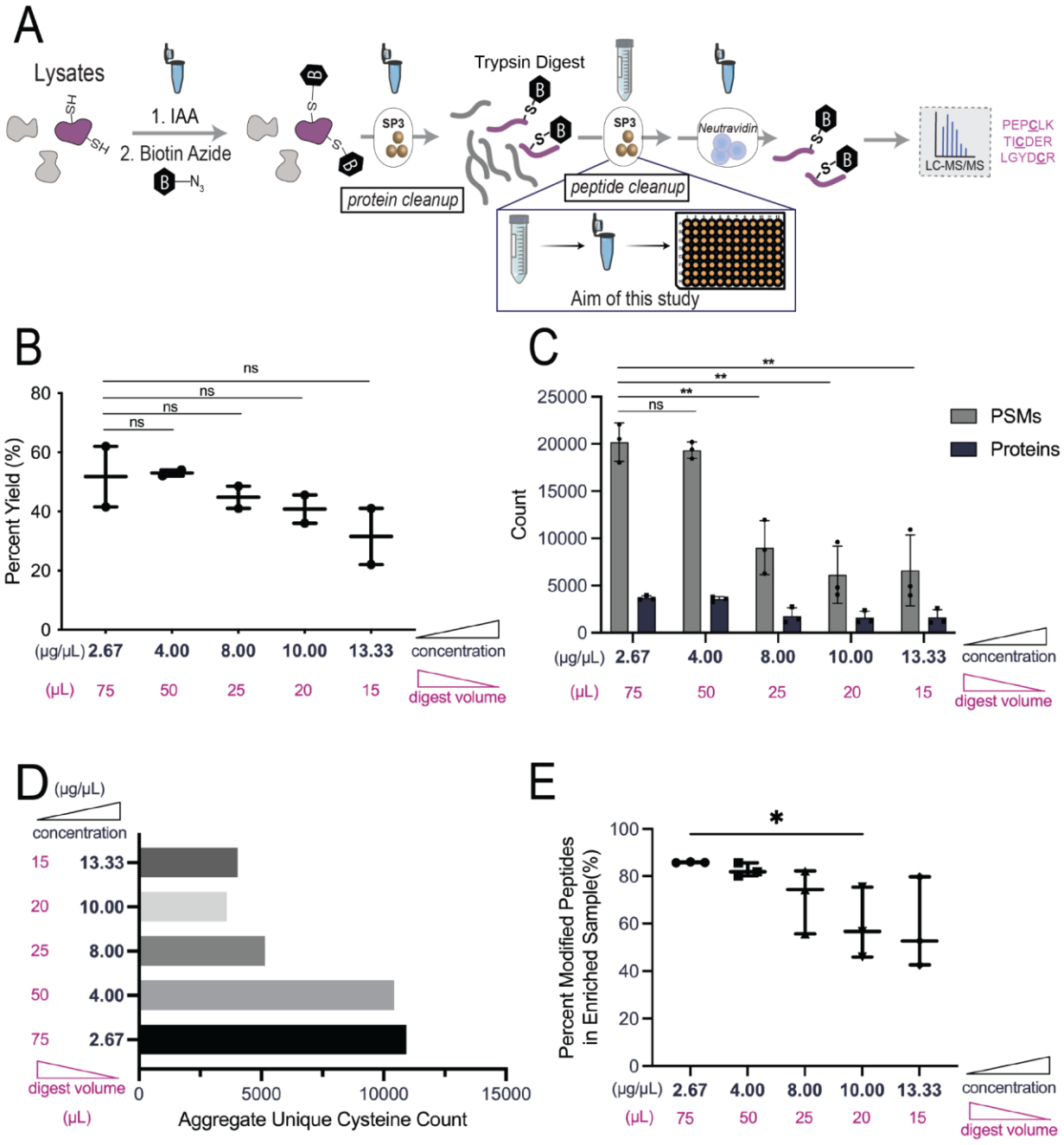

Figure 1. SP3 peptide cleanup volume scaledown results in overall decreased coverage. **A)** Shows v1.0 cysteine chemoproteomics workflow in which SP3 resin is used for both protein-

https://doi.org/10.26434/chemrxiv-2024-jm4n0 **ORCID:** https://orcid.org/0000-0001-8541-1404 Content not peer-reviewed by ChemRxiv. **License:** CC BY-NC-ND 4.0

and peptide-level sample cleanup, with scaledown of trypsin digestion sample volume to achieve compatibility with 96-well plate. **B-E)** 200 µg of Jurkat whole lysate capped with IAA and biotin azide, and subjected to v1.0 cysteine chemoproteomic sample preparation varying the trypsin digest volume and concentration. **B)** Calculated peptide recovery using peptide assay varying digest concentration and digest volume. n=2. **C)** Peptide spectral matches (PSMs) and protein coverage for digest volume scaledown. n=3. **D)** Counts of unique cysteines across all replicates (n=3) in aggregate for each digest volume used for sample preparation. **E)** Percent modified peptides in comparison to all detected peptides for each digest concentration. n=3. For B, C, E, data represent mean values and standard deviation. Statistical significance was calculated with unpaired Student's t-tests, ns, not significant, * $p<0.05$, ** $p<0.005$, NS $p>0.05$. All MS data is available in **Table S4.**

Streamlined SP3 cleanup is compatible with small molecule screening. Pleased with the overall coverage of our new and more streamlined SP3-chemoproteomic sample preparation method, we next turned to testing its utility for covalent ligand discovery. Following the workflow shown in **Figure S4**, we subjected Jurkat whole cell lysates to our benchmarking scout fragment KB2 (**Figure S2**), for which we[3,40,71] and others[4,21,22,68] have generated many high coverage prior datasets. For quantitative chemoproteomic target engagement analysis, we utilized isotopically labeled (heavy and light) biotin azide enrichment tags that can be easily clicked to IAA (**Figure S1**), enriched on neutravidin resin, and eluted from the resin under mild acid conditions. These tags have been shown to provide reliable ratios when used for quantification[38]. We tested both our biotin azide-based activity protein profiling (ABPP) under the workflow v1.0 cysteine chemoproteomic conditions (**Figure 1A**) and our newly optimized workflow v2.0 (**Figure 2A**) in parallel to further evaluate the scope of our newly modified cleanup strategy in the context of cysteine chemoproteomics (**Figure S4**). We observe similar coverage to our prior studies for both methods, with high overlap in coverage (74% of identified cysteines shared) (**Figure S5**) as well as similar ligandability profiles (**Figure S6A,B**) and types of cysteines captured (as annotated by CysDB) (**Figure S6C, S6D**). We observe generally strong concordance between liganded cysteines identified between both workflows (**Figure 2E**) and those previously reported as engaged by KB2, both for our group's prior datasets and for those generated more broadly, as reported by CysDB[68] (**Figure 2F** and **Figure S6**).

To assess whether our newly modified SP3 workflow is also compatible with other reagents besides our isotopically tagged biotin azide capture reagents, we compared them against isotopic Tandem Orthogonal Proteolysis-ABPP (isoTOP-ABPP) tobacco-etch virus (TEV) cleavable biotin reagents[5] and MS1 compatible silane-based cleavable isotopically labeled proteomic (sCIP) reagents[40] using the same electrophile KB2. Both reagents require streptavidin enrichment followed by either TEV or acid-assisted cleavage from the resin. We observed similar cysteine coverage across all reagents (**Figure S7**), illustrating the generalizability of this workflow to various custom capture reagents and enrichment types.

https://doi.org/10.26434/chemrxiv-2024-jm4n0 **ORCID:** https://orcid.org/0000-0001-8541-1404 Content not peer-reviewed by ChemRxiv. **License:** CC BY-NC-ND 4.0

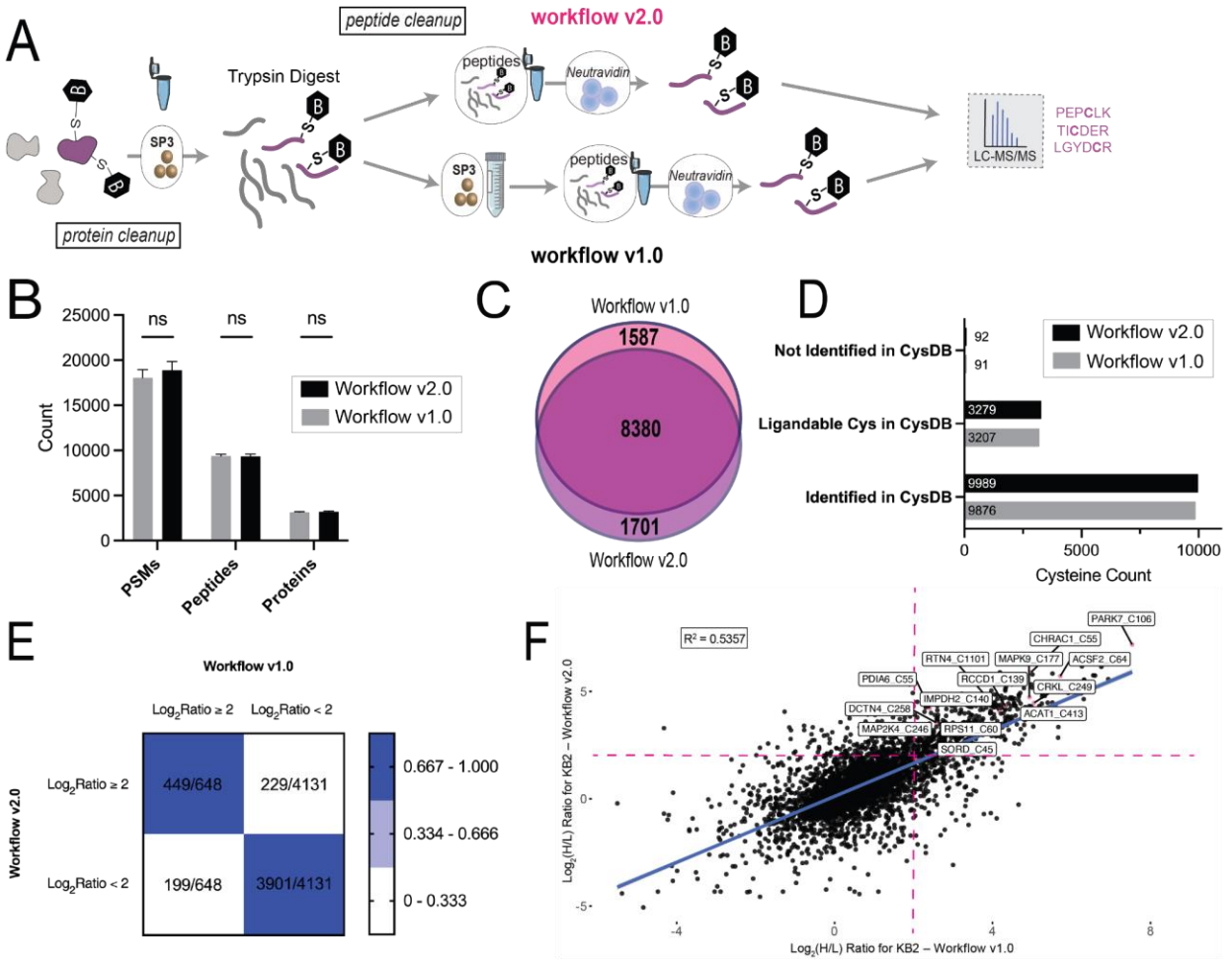

Figure 2. Skipping peptide cleanup results in comparable sample coverage and a more streamlined sample enrichment. A) Shows comparison of v1.0 **to** v2.0 workflows, with the latter omitting SP3 peptide cleanup post-digestion. Instead, in v2.0 the tryptic digest is immediately enriched onto avidin beads without extra cleanup steps. **B-D)** Jurkat whole cell lysate (400 µg) in microcentrifuge tubes labeled with IAA (200 µM) and clicked to biotin-azide processed using either workflow. n=3 per condition. **B)** Comparison of labeled PSM, peptide, and protein coverage between workflow v1.0 and workflow v2.0. **C)** Aggregate unique and shared cysteines across three replicates for each workflow. **D)** Comparison of coverage to CysDB, including both identified and ligandable unique cysteines. **E,F**) Jurkat whole cell lysate (400 µg) in microcentrifuge tubes treated with either KB2 (500 µM) or vehicle followed by IAA (200 µM), clicked to biotin-azide, and processed using either workflow, n=4 per condition. **E)** Concordance plot comparing distribution of Log_2(H/L) ratios for workflows v1.0 and 2.0 for KB2-treated Jurkat whole cell lysates. Cysteine identifiers found in more than one replicate in both workflows considered. **F)** Concordance of ligandability ratios for each workflow for KB2-treated Jurkat whole cell lysates with highlighted known KB2 liganded cysteines. Pink dashed lines indicate threshold for cysteine ligandability (Log_2HL ratio ≥ 2). Cysteine identifiers found in more than 1 replicate in both workflows considered. For B, data represent mean values and standard deviation. Statistical significance was calculated with unpaired Student's t-tests, ns, not significant $p > 0.05$. All MS data is available in **Table S5.**

https://doi.org/10.26434/chemrxiv-2024-jm4n0 **ORCID:** https://orcid.org/0000-0001-8541-1404 Content not peer-reviewed by ChemRxiv. **License:** CC BY-NC-ND 4.0

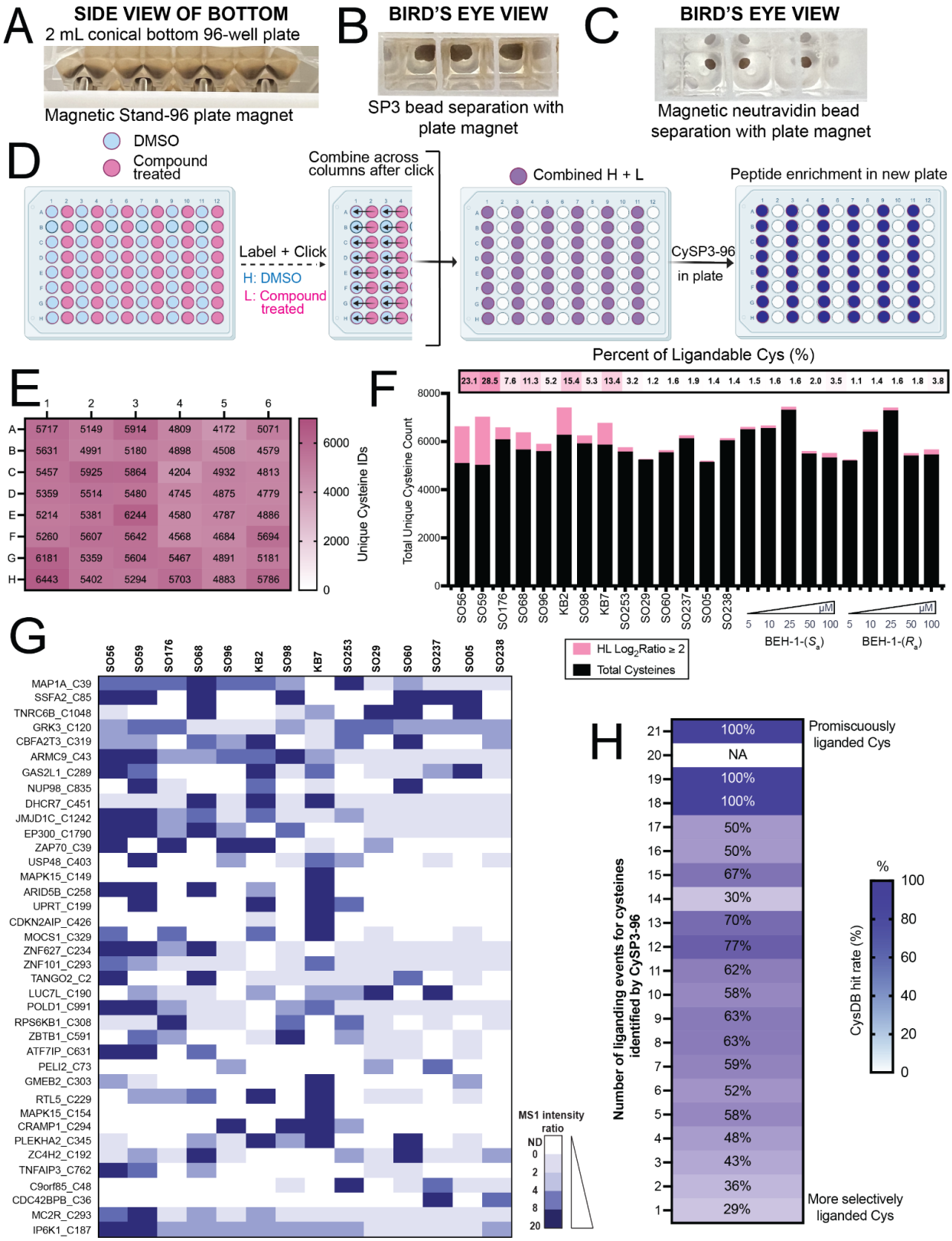

https://doi.org/10.26434/chemrxiv-2024-jm4n0 **ORCID:** https://orcid.org/0000-0001-8541-1404 Content not peer-reviewed by ChemRxiv. **License:** CC BY-NC-ND 4.0

Figure 3. Streamlined SP3 preparation seamlessly transitions into 96 deep well plate format for screening of cysteine reactive electrophiles. A) Deep-well plate with Magnetic Stand-96 magnet used for bead separation. **B)** Visualization of the magnetic bead separation in each well. **C)** Visualization of Cytiva magnetic neutravidin bead separation in each well for enrichment. **D)** Workflow for the plate-based screening starting with in-plate lysate treatment with compounds or vehicle, labeling with IAA, click conjugate to either heavy or light biotin azide enrichment reagents, and proteomic sample preparation. **E)** Number of unique cysteines identified per well across the plate for cysteine electrophilic compound screen. **F)** Cysteine ligandability per compound as compared to overall coverage. **G)** Shows the SAR of liganded cysteines not previously identified in CysDB. **H)** Comparison of the hit rate (percentage of total compounds screened that engage a cysteine in CysDB) to the number of liganding events reported by CySP3-96, with a max of 21 liganding events for the 16 compounds screened, including dose response assessments. For panels E-H, Jurkat whole cell lysate (300 µg) in 96-well plate treated with either compound (500 µM unless otherwise stated) or vehicle followed by IAA (200 µM), clicked to either light or heavy biotin-azide, and processed via chemoproteomics workflow v2.0, n=2 per condition. All MS data is available in **Table S6**.

Transitioning our enhanced SP3 method into a 96-well plate format. The key overarching goal of our study was to achieve streamlined well-plate sample preparation, with a particular focus on compatibility with large sample inputs that are not amenable to the state-of-the-art SP3-TMT methods[21,39]. Therefore, our next step was to transition our method from 1.5 mL microcentrifuge tubes to a 96-well plate. To enable compatibility with >200 µg sample input, we selected a 2 mL deep well plate as the optimal container to match anticipated workflow volumes (**Table S2**). We then purchased two models of plate (round U-bottom and conical V-bottom) and compared capture of SP3 resin by two widely used magnets[72–74], Magnetic Stand-96 versus DynaMag 96. We find that the conical bottom plates paired with the Magnetic Stand-96 afford improved ease of handling and similar coverage as compared to other options assessed (**Figure S8)**. Visual inspection rationalized the increased performance of the Magnetic Stand-96, which features round magnets, compared to the DynaMag 96 side skirted plate magnet, with the former affording improved SP3 resin capture (**Figure 3A-C** and **Figure S8**). We attribute this to the increased spacing in the conical V-bottom plates which allow for the round magnets in the Magnetic Stand-96 to sit higher up the side of the well as compared to the DynaMag 96. Lastly, our choice of plate was also guided by compatibility with reusable plate seals that are compatible with the vigorous shaking steps in the SP3 workflow.

Benchmarking against our microcentrifuge-based approach revealed comparable cysteine chemoproteomic coverage for our newly established well-plate-based platform (**Figure S9A-C**). Further illustrating the robustness of our method, we find that similar coverage was observed for enrichment on magnetic neutravidin, with magnet-based resin cleanup, compared to conventional neutravidin, with centrifugation-based cleanup (**Figure S9A-C**). Notably, this advance allows for full plate-based sample preparation, which substantially minimizes both manual sample manipulation and preparation time.

Showcasing the versatility of our approach, we observe high coverage of cysteine peptides across a range of protein inputs, spanning 100-800 µg, with a slight decrease in

https://doi.org/10.26434/chemrxiv-2024-jm4n0 **ORCID:** https://orcid.org/0000-0001-8541-1404 Content not peer-reviewed by ChemRxiv. **License:** CC BY-NC-ND 4.0

coverage at lower 50 µg input amounts (**Figure S10A**). While this plate-based platform is compatible with larger volumes, for cysteine chemoproteomics 200 µg proved sufficient to achieve high coverage (**Figure S10A,B**). We note that the compatibility of our method with larger volumes could be useful for studies using less reactive probes[66]. These findings align with our prior report for down-scaling of microcentrifuge-based sample preparation[41], and we expect that, when paired with isobaric multiplexing, further scale down should be feasible, consistent with the recent report by Gygi and coworkers[39]. Additionally, when compared to more dilute chemoproteomic samples, we observed that higher concentration and lower volume samples afforded a modest increase in coverage (**Figure S10B**), which further highlights the value of our reduced volume approach.

CySP3-96 enables rapid screening of focused sets of cysteine-reactive electrophilic compounds. With our plate-based method established, we next opted to deploy our approach to screen a focused library of cysteine reactive electrophiles in Jurkat whole cell lysates. We assembled a panel of two previously screened electrophilic compounds, the aforementioned KB2 together with KB7[3,40,71], and 12 newly synthesized fragment-like molecules that span a range of electrophilic chemotypes (**Figure S1**). We additionally included two more elaborated atropisomeric compounds into our screening library (BEH-1-(S_a) and BEH-1-(R_a)), which were designed based on the covalent HER2 and EGFR kinase inhibitor neratinib that is used to treat HER2+ breast cancer and synthesized in 25% yield (**Scheme 1**).

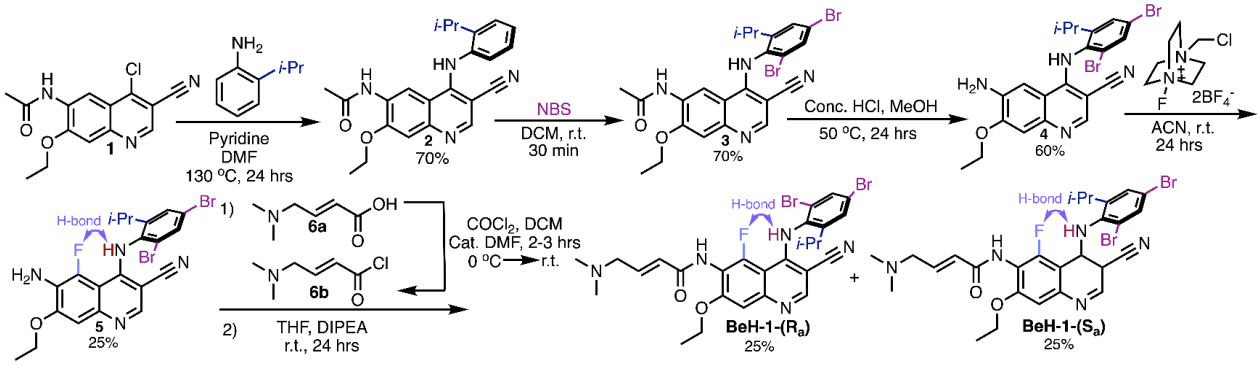

Scheme 1. Synthesis of atropisomeric compounds.

Then, following the scheme shown in **Figure 3D**, we subjected Jurkat whole cell lysates to each compound or DMSO vehicle. Following compound incubation and click conjugation to isotopically enriched biotin-azide capture reagents, the samples were combined pairwise across the plate to generate 48 unique samples for competitive chemoproteomic analysis (**Figure S4** workflow). To further showcase the versatility of our workflow and to better pinpoint high affinity targets, we also generated dose-response datasets, screening BEH-1-(S_a) and BEH-1-(R_a) at a range of compound concentrations spanning 5 µM to 100 µM. In total, across all datasets, 12265 unique cysteines from 4375 proteins were quantified. This coverage is comparable to that reported for other recent high coverage chemoproteomic screening platforms[21,75]. Coverage was highly consistent across all wells and compounds analyzed (**Figure 3E,F** and **Figure S11**),

https://doi.org/10.26434/chemrxiv-2024-jm4n0 **ORCID:** https://orcid.org/0000-0001-8541-1404 Content not peer-reviewed by ChemRxiv. **License:** CC BY-NC-ND 4.0

illustrating that the CySP3-96 workflow does not introduce plate position-based biases or other significant sources of variability.

Prior studies have revealed that apparent cysteine-reactivity can vary considerably across different electrophiles and compounds of varying electronics and lipophilicities[1,3]. Therefore, we next assessed the relative compound reactivity, as inferred from the fraction of cysteines liganded (Log_2(H/L) ≥ 2). We find that the topmost reactive compounds are SO56 and SO59, which have the same scaffold and adduct 23% and 28% of identified cysteines (**Figure 3F**). By contrast, most other compounds (other than KB2 and KB7) showed attenuated reactivity <12%, including the two atropisomeric compounds. To further corroborate these findings, we performed gel-based analysis and assessed the relative competition of IARho labeling by each compound, which revealed labeling patterns generally consistent with our calculated proteomic reactivity (**Figure S12**). Thus CySP3-96 can capture the relative reactivity of different cysteine reactive electrophiles across the proteome.

To further vet our CySP3-96 screening data, we compared the liganded cysteines (Log2(H/L) ≥ 2) identified for widely used compounds, KB2 and KB7, to those identified previously. We observe a number of shared targets, including MAPK9 Cys177 for KB7 and KB2 (**Figure S13**). Looking more broadly across our data, we identified 2280 total ligandable cysteines across all compounds screened. A number of highly ligandable cysteines stand out, including Cys1101 in RTN4 and Cys114 in TIGAR (**Figure S13**), which are also identified as very ligandable by prior studies[3,68]. These examples illustrate the capacity of CySP3-96 to identify bona fide cysteine labeling sites. Additionally, we found a strong concordance for the ratios measured for KB2 samples prepared in microfuge tubes using workflow v1.0 to the KB2 samples generated in the 96-well plate (**Figure S14**). Looking beyond these well characterized cysteines, we were also pleased to observe that our dataset captured 607 cysteines not previously identified in CysDB (**Figure 3H**), including Cys 120 in GRK3, Cys 835 in NUP98, and Cys 403 in USP48. Further looking into the types of cysteines not previously seen in CysDB, we find that 24% of the new cysteines belonging to proteins with transcription factor and/or regulator functions are liganded by 2 or more compounds (**Figure S15**). The next most liganded groups were the proteins classified under the enzyme group, the scaffolding, modulator, adaptor group, and the uncategorized group, each containing 17% of the cysteines in the group to be liganded by 2 or more of the compounds used for screening (**Figure S15**). We ascribe its newfound ligandability both to the novel compounds in our screening library together with the robust coverage afforded by our CySP3-96 platform. Taken together these examples illustrate the capacity of CySP3-96 to identify established and novel ligandable cysteines and to enable high coverage screening of focused electrophilic libraries.

Atropisomeric electrophiles show distinct proteome-wide SAR. As atropisomers feature conformationally constrained chiral bonds[76], we hypothesized that BEH-1-(S_a) and BEH-1-(R_a) compounds would each engage unique cysteines. To test this hypothesis, we first stratified the cysteine ligandability ratios across the concentration range screened for each compound and compared the ratios obtained for the BEH-1-(S_a) and BEH-1-(R_a) compounds (**Figure 4A**). Consistent with our hypothesis, we find that 66 total cysteines are preferentially labeled by one atropisomer. Of these, 30 cysteines had not been found to be ligandable in CysDB, which are

https://doi.org/10.26434/chemrxiv-2024-jm4n0 **ORCID:** https://orcid.org/0000-0001-8541-1404 Content not peer-reviewed by ChemRxiv. **License:** CC BY-NC-ND 4.0

highlighted with bolded identifiers in **Figure 4B**. As the general reactivity of each compound was observed to be comparable (**Figure 3F**), we expected that these differences were reflective of bona fide SAR.

These newly liganded cysteine proteins include DNA/RNA binding proteins, such as Cys208 in NONO and Cys169 in EIF3G. We were also pleased to observe that both atropisomers engaged many kinase cysteines, including residues such as Cys317 in UCKL1 (S_a), Cys9 in STK38 (S_a), and Cys340 in GRK2 (R_a). This observation aligns with the nature of these compounds as analogues of known kinase inhibitors. Further highlighting enantioselective SAR reported by our platform, we find that BEH-1-(S_a) shows increased labeling of transferase/kinase annotated proteins as compared to BEH-1-(R_a) (**Figure S16**). Illustrating this activity, we see that the active-site adjacent CAMK4 Cys202 was preferentially engaged by BEH-1-(S_a) (**Figure 4B**). Highlighting possibilities for distinct binding modes, we observed that Cys231 in the kinase CHEK2 was preferentially engaged by BEH-1-(R_a), particularly at lower compound concentrations (**Figure 4B**). These compelling examples illustrate the utility of screening atropisomeric compounds for target hunting. We do also note that we did not identify cysteines from the neratinib targets EGFR and HER2, likely due to very low levels of protein expression in Jurkat cells and the lack of inhibition of these kinases observed for BEH-1-(S_a) and BEH-1-(R_a), in an established kinase activity assay (**Figure S17).**

Intrigued by the preferential labeling of CHEK2 by *R* atropisomer, we next subjected CHEK2 (PDB ID: 2XBJ) to non-covalent molecular docking with Molecular Operating Environment (MOE) software using a cutoff distance of 6 angstroms for energy minimization calculation, with the goal of assessing whether the chemoproteomic data could be corroborated in silico. Consistent with the chemoproteomic-preference for BEH-1-(R_a), we find that most (4/5) of the binding poses observed for BEH-1 adopt the R conformation (**Figure 4C** and **Figure S18)**. The best R enantiomer binding pose was also observed to exhibit the lowest overall binding energy, with an MOE predicted affinity score of -5.0164 (**Figure 4C**). In addition to the covalent linkage, multiple contacts were observed between CHEK2 and the BEH-1-(R_a) atropisomer within this pocket (**Figure 4E-F**). Taken together, these docking studies corroborate the chemoproteomic reported enantioselective labeling at CHEK2.

https://doi.org/10.26434/chemrxiv-2024-jm4n0 **ORCID:** https://orcid.org/0000-0001-8541-1404 Content not peer-reviewed by ChemRxiv. **License:** CC BY-NC-ND 4.0

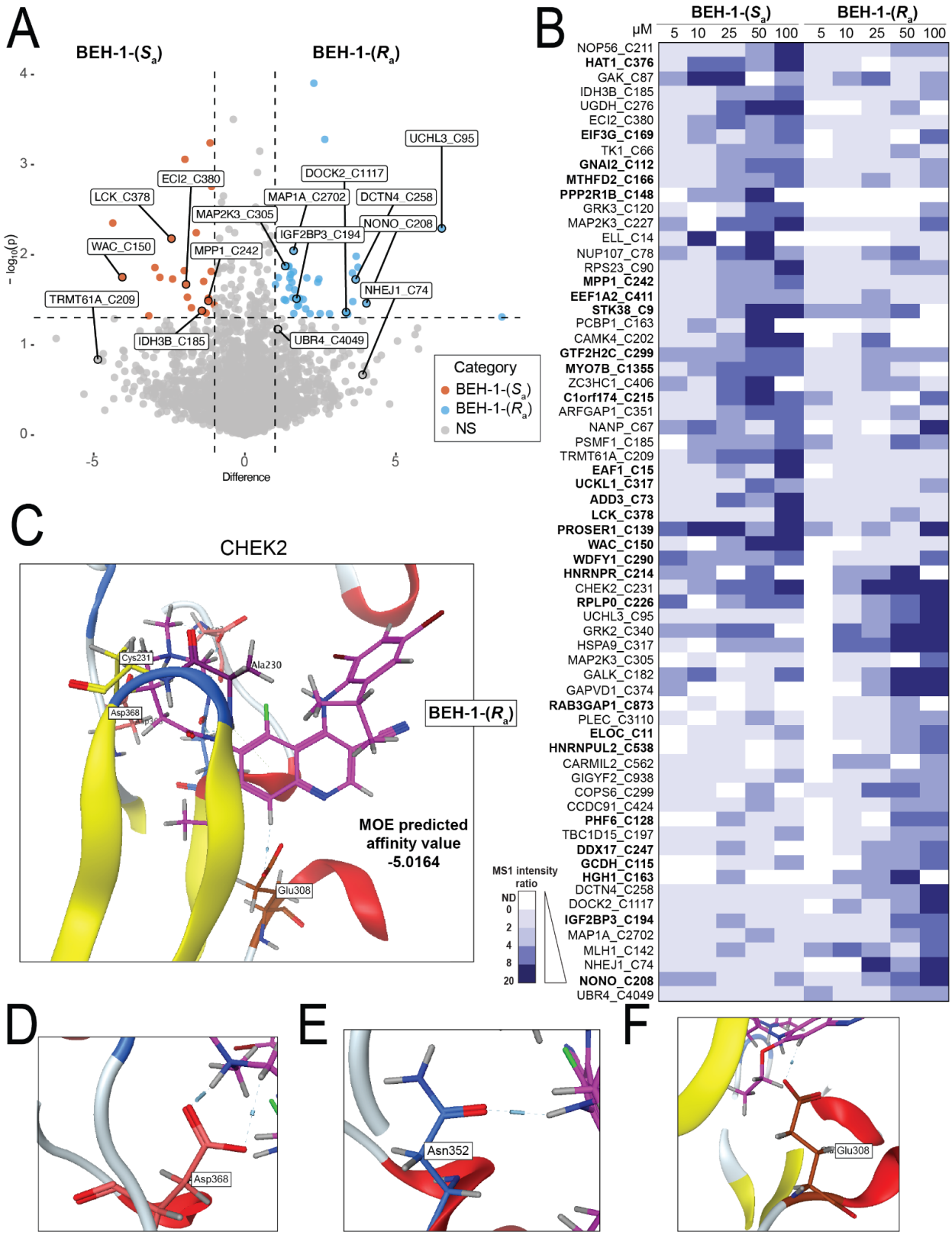

https://doi.org/10.26434/chemrxiv-2024-jm4n0 **ORCID:** https://orcid.org/0000-0001-8541-1404 Content not peer-reviewed by ChemRxiv. **License:** CC BY-NC-ND 4.0

Figure 4. Concentration screen of two atropisomers BEH-1-(S_a) and BEH-1-(R_a) illustrates stereoselectivity across targets. A,B) Jurkat whole cell lysate (300 µg) in 96-well plate treated with either BEH-1-(S_a) and BEH-1-(R_a) at the indicated concentration or vehicle followed by IAA (200 µM), clicked to either light or heavy biotin-azide, and processed via chemoproteomics workflow v2.0, n=2 per condition. **A)** Volcano plot of the fold change difference of the Log_2(H/L) ratios for Jurkat whole cell lysates treated with BEH-1-(S_a) and BEH-1-(R_a) (100 µM) followed by cysteine chemoproteomic analysis. **B)** Heatmap of atropisomer targets across a range of concentrations between 5 and 100 µM. Bolded sites indicate those not previously identified as ligandable in CysDB. **C)** CHEK2 (PDB ID: 2XBJ) Cys231 docked to BEH-1-(R_a) with an MOE predicted affinity value of -5.0164. Four out of five poses observed with BEH-1-(R_a) atropisomer. **D)** A zoom in of C: Asp368 in the hinge region of CHEK2 making hydrogen bonding interactions with the dimethylamino moiety of BEH-1-(R_a) as well as its adjacent CH_2 group. **E)** A zoom in of C: Asn352 in the hinge region of CHEK2 making a hydrogen bond with the hydrogen of the amine group in the covalent linker moiety of BEH-1-(R_a). **F)** A zoom in of C: Glu308 in the hinge region of CHEK2 making a hydrogen bond with the C8 hydrogen of the quinoline moiety of BEH-1-(R_a). All docking figures generated with CHEK2 PDB structure 2XBJ in MOE 2020. All MS data is available in **Table S6.**

Establishing a low-cost option for magnetic bead-based sample cleanup. Achieving cost savings was a key goal of our study. Therefore, we next sought to identify budget friendly SP3 resin. We were inspired by recent studies that had shown, for protein cleanup, low cost glass beads function comparably to higher cost magnetic resin[77], albeit using centrifugation to isolate the resin. Other studies have also shown that the surface chemistry of beads is largely irrelevant to sample preparation, which is facilitated by protein precipitation rather than true binding to beads[78]. Thus, we hypothesized that other low-cost magnetic resins would function comparable to the widely used Cytiva resin. To test this hypothesis, we selected a low cost commercially available resin sold by Sergi Lab Supplies as a reagent for oligonucleotide cleanup (**Figure 5A**). Visual inspection of the appearance of each resin slurry revealed that the low cost resin appeared more dilute, which was confirmed by the lower compacted bead volume (approximately 1/5th the size for the same volume taken, upon visual inspection) (**Figure 5B,C**). Thus, we opted to adjust the volume of slurry used to match the compacted bead volume between the two resins for our initial proteomic sample preparation. Gratifyingly, head-to-head chemoproteomic coverage comparison revealed no significant difference in coverage between the two resins (**Figure 5D**).

As the scaled-up slurry volume would diminish the potential cost-savings, we also tested the performance of lower slurry volumes (**Figure S19)**. We find the coverage is unchanged when the magnetic beads were used in the same ratio as the SP3 beads: 1 µg of protein to 10 µL of slurry (**Figure 5D** and **Figure S19**). Visual inspection of these samples revealed a striking advantage of the low-cost resin: the smaller bead volume of the magnetic beads allows for more space within the well for aspirating supernatant throughout this workflow (**Figure 5B**). The low bead volume also afforded a visual cue of efficient protein capture, namely an increase in the whitish hue of resin that occurs after protein precipitation **(Figure 5C**). As a note of caution, we do acknowledge that ultra-low resin volumes (<40 µL bead slurry), particularly for small volume samples, may result in protein pellets that are challenging to visualize. Therefore, we do not recommend using bead slurry volumes of less than 40 µL.

https://doi.org/10.26434/chemrxiv-2024-jm4n0 **ORCID:** https://orcid.org/0000-0001-8541-1404 Content not peer-reviewed by ChemRxiv. **License:** CC BY-NC-ND 4.0

To further vet this resin, we also compared coverage of cysteines identified. We find that >80% of cysteines are captured by both resins with no significant difference in classes of proteins observed for each resin (**Figure 5E,F**). We ascribe the handful of cysteines preferentially identified by each resin to the stochastic nature of DDA, although we cannot rule out differences in resin affinities. Lastly, we also assessed whether this new resin could also prove useful for peptide-level sample cleanup post-tryptic digest—while not required for the CySP3-96 method, peptide cleanup is highly useful for other methods, such our redox proteomic platform SP3-Rox[43]. We find comparable peptide recovery is achieved for both resins analyzed (**Figure S20**). In sum, these data provide compelling evidence of the general utility of the Sergi Lab Supplies resin, which affords savings of >85% across 750 sample preparations equates to over $1300 (**Figure 5A**).

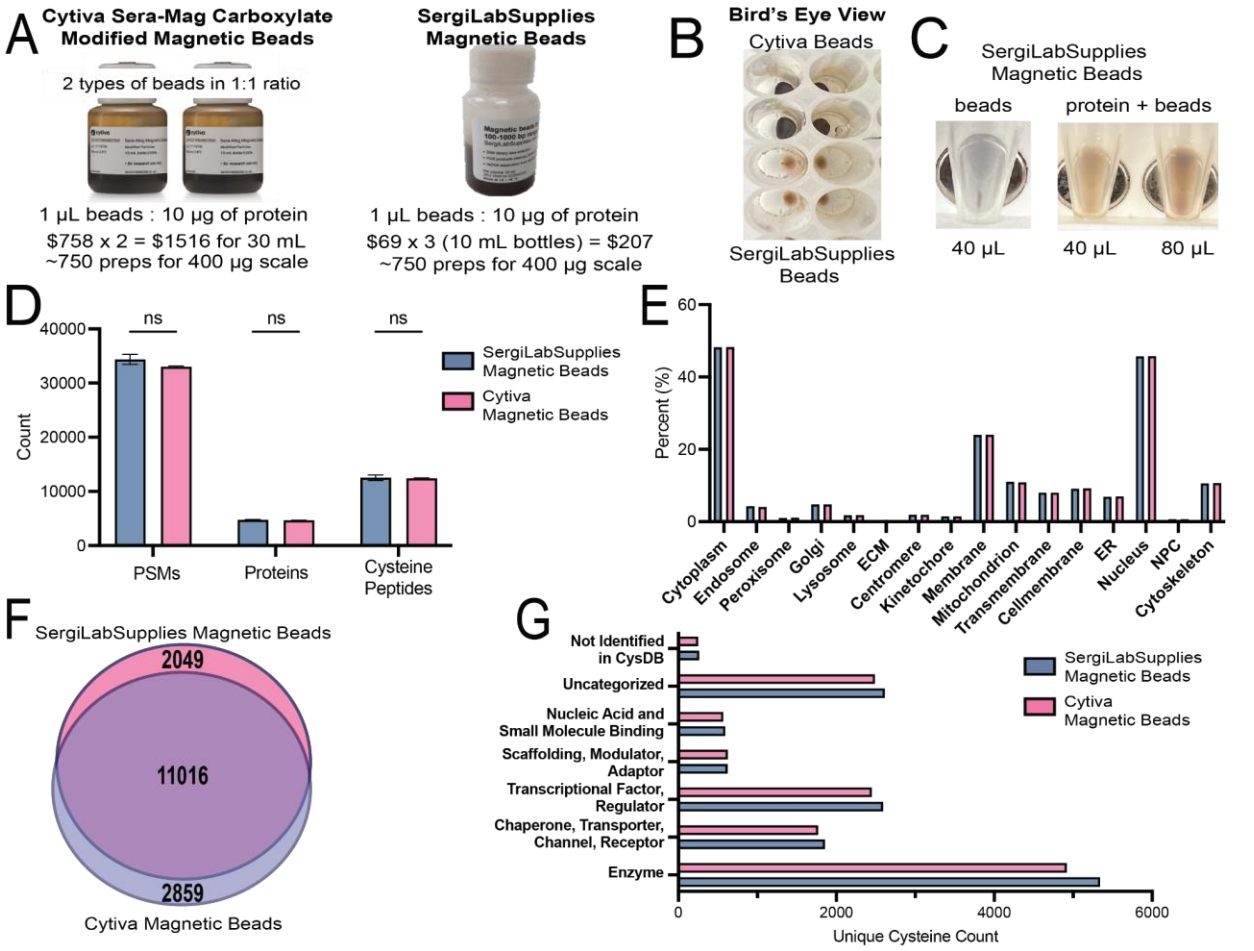

Figure 5. **Identifying a low-cost magnetic option for SP3. A)** Cost analysis of using Cytiva's SP3 beads versus SergiLabSupplies magnetic beads usually used for oligonucleotide purification. **B)** Shows deep-well plate setup with SergiLabSupplies magnetic beads (bottom 2 rows) or Cytiva's SP3 beads (top two rows) to show differences in bead volume. Smaller bead volumes allow for more free space for tips when aspirating washes. **C)** Shows SergiLabSupplies magnetic beads without protein and when protein is immobilized onto beads. **D)** Comparison of PSM,

https://doi.org/10.26434/chemrxiv-2024-jm4n0 **ORCID:** https://orcid.org/0000-0001-8541-1404 Content not peer-reviewed by ChemRxiv. **License:** CC BY-NC-ND 4.0

protein, and cysteine coverage between the same volume of SergiLabSupplies magnetic beads as compared to Cytiva's SP3 beads, n=2. **E)** Classes of proteins detected, based upon UniProtKB annotations, from sample preparations using the magnetic beads or SP3 beads. **F)** Overlap of unique cysteines identified by each bead type. **G)** Categorization of each cysteine identifier from CysDB for each bead type. Statistical significance was calculated by performing an unpaired Student's t-test. $p < 0.05$ for significance cutoff. All MS data is available in **Table S7**.

Discussion

In this study we developed a 96-well SP3 workflow, CySP3-96, for the high throughput processing of chemoproteomic samples. Taken together CySP3-96 chemoproteomics performed comparably to other cutting-edge platforms, identifying in aggregate 12265 unique cysteines, of which 607 had not been previously captured by CysDB.

To establish CySP3-96, we first address the scalability limitation of SP3, to enable sample preparations with large amounts of input material. We expect that this methodological innovation should prove particularly useful for applications where coverage is tightly linked to sample amount, such as chemoproteomics using less reactive probes. Likely the scalability of our approach will also prove beneficial in addition to workflows that pool samples at the protein level, thereby increasing sample amount per experiment. Such applications include for cysteine redox proteomics (SP3-Rox)[43] and for isobaric labeling studies using our sCIP reagents[40].

After extensive benchmarking to ensure the robustness of our plate-based workflow, we deployed our platform to screen a focused library of cysteine-reactive electrophilic compounds. Our screening library contains both previously reported and novel electrophilic compounds, including an elaborated pair of atropisomeric analogues of neratinib. In aggregate we identify 2280 ligandable cysteines, including 67 residues with atropisomeric selectivity. As demonstrated by recent work using stereoprobe libraries[45], we expect that atropisomeric compounds should prove similarly useful in guiding the discovery of high confidence and actionable cysteine-compound pairs.

The increased sample throughput offered by CySP3-96 (between 1.5h to 12h decreased active sample manipulation time, **Figure S21**), facilitates testing dose-response across a range of compound concentrations. As shown for the pair of atropisomeric compounds tested here, testing a range of compound concentrations is valuable for delineation of high versus low affinity labeling events. We expect that dose ranges should also prove useful for delineating on-target labeling from compound-induced changes to protein abundance caused by generalized cell stress—of note, our recent work revealed that many electrophilic compounds activate cellular stress responses, including stress granules and aggresomes when compound concentrations exceed low micromolar concentrations[71].

Looking beyond chemoproteomics, we expect that our low-cost magnetic resin-based scalable high throughput cleanup workflow should prove useful for a wide range of applications that require increased sample input as well as increased number of samples. Our envisioned applications include for SP3-based phosphoproteomics workflows[62], SP3-based immunopeptidomics[79], and for upscaling for microflow-based sample separation[55,67]. Lastly, building on prior reports that revealed the surface chemistry flexibility of bead-based peptide

https://doi.org/10.26434/chemrxiv-2024-jm4n0 **ORCID:** https://orcid.org/0000-0001-8541-1404 Content not peer-reviewed by ChemRxiv. **License:** CC BY-NC-ND 4.0

cleanup, we anticipate that a range of magnetic resins will likely function comparable for both protein- and peptide-based sample decontamination.

Author Contributions

F.S, and K.M.B. conceived of the project. F.S., and K.M.B designed experiments. F.S., B.S.H., J.D., C.T., A.C.T., and L.H. collected data. B.S.H. and S.O. performed synthesis. F.S. and B.S.H. performed data analysis. F.S. contributed to the figures. F.S and K.M.B. wrote the manuscript with assistance from all authors.

Conflicts of Interest

K.M.B. is a member of the advisory board at Matchpoint Therapeutics.

Acknowledgements

This study was supported by a Beckman Young Investigator Award (K.M.B.) and Ono Pharma Breakthrough Science Initiative Innovation Award (K.M.B). We additionally thank all members of the Backus lab members for helpful suggestions.

Proteomic data availability. The MS data have been deposited to the ProteomeXchange Consortium via the PRIDE partner repository[80] with the dataset identifier PXD054043. File details can be found in **Table S8**.

Code Availability. The scripts used for this work are available at https://github.com/BackusLab.

References

1. Zanon, P. R. A. *et al.* Profiling the Proteome-Wide Selectivity of Diverse Electrophiles. (2021) doi:10.26434/chemrxiv.14186561.v1.

2. Lin, Z. *et al.* Activity-Based Hydrazine Probes for Protein Profiling of Electrophilic Functionality in Therapeutic Targets. *ACS Cent. Sci.* **7**, 1524–1534 (2021).

3. Backus, K. M. *et al.* Proteome-wide covalent ligand discovery in native biological systems. *Nature* **534**, 570–574 (2016).

4. Takahashi, M. *et al.* DrugMap: A quantitative pan-cancer analysis of cysteine ligandability. *Cell* **187**, 2536-2556.e30 (2024).

5. Weerapana, E. *et al.* Quantitative reactivity profiling predicts functional cysteines in proteomes. *Nature* **468**, 790–795 (2010).

6. Abbasov, M. E. *et al.* A proteome-wide atlas of lysine-reactive chemistry. *Nat. Chem.* **13**, 1081–1092 (2021).

https://doi.org/10.26434/chemrxiv-2024-jm4n0 **ORCID:** https://orcid.org/0000-0001-8541-1404 Content not peer-reviewed by ChemRxiv. **License:** CC BY-NC-ND 4.0

7. Hacker, S. M. *et al.* Global profiling of lysine reactivity and ligandability in the human proteome. *Nat. Chem.* **9**, 1181–1190 (2017).

8. Simon, G. M. & Cravatt, B. F. Activity-based proteomics of enzyme superfamilies: serine hydrolases as a case study. *J. Biol. Chem.* **285**, 11051–11055 (2010).

9. Shenoy, V. M. *et al.* Chemoproteomic Identification of Serine Hydrolase RBBP9 as a Valacyclovir-Activating Enzyme. *Mol. Pharm.* **17**, 1706–1714 (2020).

10. Li, W., Blankman, J. L. & Cravatt, B. F. A functional proteomic strategy to discover inhibitors for uncharacterized hydrolases. *J. Am. Chem. Soc.* **129**, 9594–9595 (2007).

11. Chen, Y. *et al.* Direct mapping of ligandable tyrosines and lysines in cells with chiral sulfonyl fluoride probes. *Nat. Chem.* **15**, 1616–1625 (2023).

12. Hahm, H. S. *et al.* Global targeting of functional tyrosines using sulfur-triazole exchange chemistry. *Nat. Chem. Biol.* **16**, 150–159 (2020).

13. Mortenson, D. E. *et al.* "inverse drug discovery" strategy to identify proteins that are targeted by latent electrophiles as exemplified by aryl fluorosulfates. *J. Am. Chem. Soc.* **140**, 200–210 (2018).

14. Lin, S. *et al.* Redox-based reagents for chemoselective methionine bioconjugation. *Science* **355**, 597–602 (2017).

15. Gonzalez-Valero, A. *et al.* An Activity-Based Oxaziridine Platform for Identifying and Developing Covalent Ligands for Functional Allosteric Methionine Sites: Redox-Dependent Inhibition of Cyclin-Dependent Kinase 4. *J. Am. Chem. Soc.* **144**, 22890–22901 (2022).

16. Bach, K., Beerkens, B. L. H., Zanon, P. R. A. & Hacker, S. M. Light-Activatable, 2,5-Disubstituted Tetrazoles for the Proteome-wide Profiling of Aspartates and Glutamates in Living Bacteria. *ACS Cent. Sci.* **6**, 546–554 (2020).

17. Ma, N. *et al.* 2H-Azirine-Based Reagents for Chemoselective Bioconjugation at Carboxyl Residues Inside Live Cells. *J. Am. Chem. Soc.* **142**, 6051–6059 (2020).

18. Cheng, K. *et al.* Tetrazole-Based Probes for Integrated Phenotypic Screening, Affinity-Based Proteome Profiling, and Sensitive Detection of a Cancer Biomarker. *Angew. Chem. Int. Ed* **56**, 15044–15048 (2017).

19. Ostrem, J. M., Peters, U., Sos, M. L., Wells, J. A. & Shokat, K. M. K-Ras(G12C) inhibitors allosterically control GTP affinity and effector interactions. *Nature* **503**, 548–551 (2013).

20. Fell, J. B. *et al.* Identification of the clinical development candidate MRTX849, a covalent KRASG12C inhibitor for the treatment of cancer. *J. Med. Chem.* **63**, 6679–6693 (2020).

https://doi.org/10.26434/chemrxiv-2024-jm4n0 **ORCID:** https://orcid.org/0000-0001-8541-1404 Content not peer-reviewed by ChemRxiv. **License:** CC BY-NC-ND 4.0

21. Kuljanin, M. *et al.* Reimagining high-throughput profiling of reactive cysteines for cell-based screening of large electrophile libraries. *Nat. Biotechnol.* **39**, 630–641 (2021).

22. Vinogradova, E. V. *et al.* An Activity-Guided Map of Electrophile-Cysteine Interactions in Primary Human T Cells. *Cell* **182**, 1009-1026.e29 (2020).

23. Bar-Peled, L. *et al.* Chemical proteomics identifies druggable vulnerabilities in a genetically defined cancer. *Cell* **171**, 696-709.e23 (2017).

24. Abegg, D. *et al.* Proteome-Wide Profiling of Targets of Cysteine reactive Small Molecules by Using Ethynyl Benziodoxolone Reagents. *Angew. Chem.* **127**, 11002–11007 (2015).

25. Grossman, E. A. *et al.* Covalent Ligand Discovery against Druggable Hotspots Targeted by Anti-cancer Natural Products. *Cell Chem. Biol.* **24**, 1368-1376.e4 (2017).

26. Wang, C., Weerapana, E., Blewett, M. M. & Cravatt, B. F. A chemoproteomic platform to quantitatively map targets of lipid-derived electrophiles. *Nat. Methods* **11**, 79–85 (2014).

27. Zambaldo, C. *et al.* 2-Sulfonylpyridines as Tunable, Cysteine-Reactive Electrophiles. *J. Am. Chem. Soc.* **142**, 8972–8979 (2020).

28. Cravatt, B. *et al.* Comprehensive Mapping of Electrophilic Small Molecule-Protein Interactions in Human Cells. (2023) doi:10.26434/chemrxiv-2023-s446n.

29. Zhang, J. *et al.* Systematic identification of anticancer drug targets reveals a nucleus-to-mitochondria ROS-sensing pathway. *Cell* **186**, 2361-2379.e25 (2023).

30. Henning, N. J. *et al.* Discovery of a covalent FEM1B recruiter for targeted protein degradation applications. *J. Am. Chem. Soc.* **144**, 701–708 (2022).

31. Henning, N. J. *et al.* Deubiquitinase-targeting chimeras for targeted protein stabilization. *Nat. Chem. Biol.* **18**, 412–421 (2022).

32. Toriki, E. S. *et al.* Rational chemical design of molecular glue degraders. *ACS Cent. Sci.* **9**, 915–926 (2023).

33. Boike, L. *et al.* Discovery of a Functional Covalent Ligand Targeting an Intrinsically Disordered Cysteine within MYC. *Cell Chem. Biol.* **28**, 4-13.e17 (2021).

34. Lazear, M. R. *et al.* Proteomic discovery of chemical probes that perturb protein complexes in human cells. *Mol. Cell* **83**, 1725-1742.e12 (2023).

35. Kathman, S. G. *et al.* Remodeling oncogenic transcriptomes by small molecules targeting NONO. *Nat. Chem. Biol.* **19**, 825–836 (2023).

36. Darabedian, N. *et al.* Depletion of creatine phosphagen energetics with a covalent creatine kinase inhibitor. *Nat. Chem. Biol.* **19**, 815–824 (2023).

https://doi.org/10.26434/chemrxiv-2024-jm4n0 **ORCID:** https://orcid.org/0000-0001-8541-1404 Content not peer-reviewed by ChemRxiv. **License:** CC BY-NC-ND 4.0

37. Shuken, S. R. *et al.* Deep Proteomic Compound Profiling with the Orbitrap Ascend Tribrid Mass Spectrometer Using Tandem Mass Tags and Real-Time Search. *Anal. Chem.* (2023) doi:10.1021/acs.analchem.3c01701.

38. Desai, H. *et al.* Multi-omic stratification of the missense variant cysteinome. *BioRxiv* (2023) doi:10.1101/2023.08.12.553095.

39. Yang, K. *et al.* Accelerating multiplexed profiling of protein-ligand interactions: High-throughput plate-based reactive cysteine profiling with minimal input. *Cell Chem. Biol.* **31**, 565-576.e4 (2024).

40. Burton, N. R. *et al.* Solid-Phase Compatible Silane-Based Cleavable Linker Enables Custom Isobaric Quantitative Chemoproteomics. *J. Am. Chem. Soc.* **145**, 21303–21318 (2023).

41. Yan, T. *et al.* SP3-FAIMS Chemoproteomics for High-Coverage Profiling of the Human Cysteinome*. *Chembiochem* **22**, 1841–1851 (2021).

42. Cao, J. *et al.* Multiplexed CuAAC Suzuki-Miyaura Labeling for Tandem Activity-Based Chemoproteomic Profiling. *Anal. Chem.* **93**, 2610–2618 (2021).

43. Desai, H. S. *et al.* SP3-Enabled Rapid and High Coverage Chemoproteomic Identification of Cell-State-Dependent Redox-Sensitive Cysteines. *Mol. Cell. Proteomics* **21**, 100218 (2022).

44. Fu, L. *et al.* Nucleophilic covalent ligand discovery for the cysteine redoxome. *Nat. Chem. Biol.* **19**, 1309–1319 (2023).

45. Won, S. J. *et al.* Redirecting the pioneering function of FOXA1 with covalent small molecules. *BioRxiv* (2024) doi:10.1101/2024.03.21.586158.

46. Castellón, J. O. *et al.* Chemoproteomics Identifies State-Dependent and Proteoform-Selective Caspase-2 Inhibitors. *J. Am. Chem. Soc.* **146**, 14972–14988 (2024).

47. Akter, S. *et al.* Chemical proteomics reveals new targets of cysteine sulfinic acid reductase. *Nat. Chem. Biol.* **14**, 995–1004 (2018).

48. Wang, Y. *et al.* Expedited mapping of the ligandable proteome using fully functionalized enantiomeric probe pairs. *Nat. Chem.* **11**, 1113–1123 (2019).

49. Liu, Z. *et al.* Proteomic ligandability maps of spirocycle acrylamide stereoprobes identify covalent ERCC3 degraders. *J. Am. Chem. Soc.* **146**, 10393–10406 (2024).

50. Feldman, H. C. *et al.* Selective inhibitors of SARM1 targeting an allosteric cysteine in the autoregulatory ARM domain. *Proc Natl Acad Sci USA* **119**, e2208457119 (2022).

51. Njomen, E. *et al.* Multi-tiered chemical proteomic maps of tryptoline acrylamide-protein interactions in cancer cells. *Nat. Chem.* (2024) doi:10.1038/s41557-024-01601-1.

https://doi.org/10.26434/chemrxiv-2024-jm4n0 **ORCID:** https://orcid.org/0000-0001-8541-1404 Content not peer-reviewed by ChemRxiv. **License:** CC BY-NC-ND 4.0

52. Basilaia, M., Chen, M. H., Secka, J. & Gustafson, J. L. Atropisomerism in the pharmaceutically relevant realm. *Acc. Chem. Res.* **55**, 2904–2919 (2022).

53. Cheng, Y. *et al.* Diversity oriented clicking delivers β-substituted alkenyl sulfonyl fluorides as covalent human neutrophil elastase inhibitors. *Proc Natl Acad Sci USA* **119**, e2208540119 (2022).

54. Waas, M., Pereckas, M., Jones Lipinski, R. A., Ashwood, C. & Gundry, R. L. SP2: Rapid and Automatable Contaminant Removal from Peptide Samples for Proteomic Analyses. *J. Proteome Res.* **18**, 1644–1656 (2019).

55. Bian, Y. *et al.* Robust, reproducible and quantitative analysis of thousands of proteomes by micro-flow LC-MS/MS. *Nat. Commun.* **11**, 157 (2020).

56. Budayeva, H. G., Ma, T. P., Wang, S., Choi, M. & Rose, C. M. Increasing the Throughput and Reproducibility of Activity-Based Proteome Profiling Studies with Hyperplexing and Intelligent Data Acquisition. *J. Proteome Res.* **23**, 2934–2947 (2024).

57. Biggs, G. S. *et al.* Robust proteome profiling of cysteine-reactive fragments using label-free chemoproteomics. *BioRxiv* (2024) doi:10.1101/2024.07.25.605137.

58. Kulak, N. A., Pichler, G., Paron, I., Nagaraj, N. & Mann, M. Minimal, encapsulated proteomic-sample processing applied to copy-number estimation in eukaryotic cells. *Nat. Methods* **11**, 319–324 (2014).

59. Zougman, A., Selby, P. J. & Banks, R. E. Suspension trapping (STrap) sample preparation method for bottom-up proteomics analysis. *Proteomics* **14**, 1006–1000 (2014).

60. Hughes, C. S. *et al.* Single-pot, solid-phase-enhanced sample preparation for proteomics experiments. *Nat. Protoc.* **14**, 68–85 (2019).

61. Moggridge, S., Sorensen, P. H., Morin, G. B. & Hughes, C. S. Extending the compatibility of the SP3 paramagnetic bead processing approach for proteomics. *J. Proteome Res.* **17**, 1730–1740 (2018).

62. Chang, A., Leutert, M., Rodriguez-Mias, R. A. & Villén, J. Automated Enrichment of Phosphotyrosine Peptides for High-Throughput Proteomics. *J. Proteome Res.* **22**, 1868–1880 (2023).

63. Müller, T. *et al.* Automated sample preparation with SP3 for low-input clinical proteomics. *Mol. Syst. Biol.* **16**, e9111 (2020).

64. Yu, Y., Bekele, S. & Pieper, R. Quick 96FASP for high throughput quantitative proteome analysis. *J. Proteomics* **166**, 1–7 (2017).

65. Sielaff, M. *et al.* Evaluation of FASP, SP3, and ist protocols for proteomic sample preparation in the low microgram range. *J. Proteome Res.* **16**, 4060–4072 (2017).

https://doi.org/10.26434/chemrxiv-2024-jm4n0 **ORCID:** https://orcid.org/0000-0001-8541-1404 Content not peer-reviewed by ChemRxiv. **License:** CC BY-NC-ND 4.0

66. Takechi, S. *et al.* Silyl ether enables high coverage chemoproteomic interaction site mapping. (2024) doi:10.26434/chemrxiv-2024-21r7b.

67. Bian, Y. *et al.* Robust Microflow LC-MS/MS for Proteome Analysis: 38 000 Runs and Counting. *Anal. Chem.* **93**, 3686–3690 (2021).

68. Boatner, L. M., Palafox, M. F., Schweppe, D. K. & Backus, K. M. CysDB: a human cysteine database based on experimental quantitative chemoproteomics. *Cell Chem. Biol.* **30**, 683-698.e3 (2023).

69. Wu, X. N. *et al.* Highly Efficient Single-Step Enrichment of Low Abundance Phosphopeptides from Plant Membrane Preparations. *Front. Plant Sci.* **8**, 1673 (2017).

70. Muneer, G., Chen, C.-S., Lee, T.-T., Chen, B.-Y. & Chen, Y.-J. A Rapid One-Pot Workflow for Sensitive Microscale Phosphoproteomics. *J. Proteome Res.* (2024) doi:10.1021/acs.jproteome.3c00862.

71. Julio, A. R. *et al.* Pervasive aggregation and depletion of host and viral proteins in response to cysteine-reactive electrophilic compounds. *BioRxiv* (2023) doi:10.1101/2023.10.30.564067.

72. Bekker-Jensen, D. B. *et al.* Rapid and site-specific deep phosphoproteome profiling by data-independent acquisition without the need for spectral libraries. *Nat. Commun.* **11**, 787 (2020).

73. Kawakami, K. *et al.* Diagnostic potential of serum extracellular vesicles expressing prostate-specific membrane antigen in urologic malignancies. *Sci. Rep.* **11**, 15000 (2021).

74. Shubin, A. V. *et al.* Blood proteome profiling using aptamer-based technology for rejection biomarker discovery in transplantation. *Sci. Data* **6**, 314 (2019).

75. Burton, N. R. & Backus, K. M. Functionalizing tandem mass tags for streamlining click-based quantitative chemoproteomics. *Commun. Chem.* **7**, 80 (2024).

76. Vaidya, S. D., Heydari, B. S., Toenjes, S. T. & Gustafson, J. L. Approaches toward Atropisomerically Stable and Conformationally Pure Diarylamines. *J. Org. Chem.* **87**, 6760–6768 (2022).

77. Johnston, H. E. *et al.* Solvent Precipitation SP3 (SP4) Enhances Recovery for Proteomics Sample Preparation without Magnetic Beads. *Anal. Chem.* **94**, 10320–10328 (2022).

78. Batth, T. S. *et al.* Protein aggregation capture on microparticles enables multipurpose proteomics sample preparation. *Mol. Cell. Proteomics* **18**, 1027–1035 (2019).

79. Stopfer, L. E., Mesfin, J. M., Joughin, B. A., Lauffenburger, D. A. & White, F. M. Multiplexed relative and absolute quantitative immunopeptidomics reveals MHC I repertoire alterations induced by CDK4/6 inhibition. *Nat. Commun.* **11**, 2760 (2020).

https://doi.org/10.26434/chemrxiv-2024-jm4n0 **ORCID:** https://orcid.org/0000-0001-8541-1404 Content not peer-reviewed by ChemRxiv. **License:** CC BY-NC-ND 4.0

80. Perez-Riverol, Y. *et al.* The PRIDE database resources in 2022: a hub for mass spectrometry-based proteomics evidences. *Nucleic Acids Res.* **50**, D543–D552 (2022).

https://doi.org/10.26434/chemrxiv-2024-jm4n0 **ORCID:** https://orcid.org/0000-0001-8541-1404 Content not peer-reviewed by ChemRxiv. **License:** CC BY-NC-ND 4.0